The International Archives of the Photogrammetry, Remote Sensing and Spatial Information Sciences, Volume XLII-3/W12-2020, 2020
2020 IEEE Latin American GRSS & ISPRS Remote Sensing Conference (LAGIRS 2020), 22–26 March 2020, Santiago, Chile

# ANALYSIS OF THE EFFICIENCY OF THE ADAPTIVE CANNY METHOD FOR THE DETECTION OF ICEBERGS AT OPEN SEA

K. A. Nemer Pelliza*[1], M. A. Pucheta [1,2]

[1] Centro de Investigación en Informática para la Ingeniería (CIII), Universidad Tecnológica Nacional, F.R.C. Argentina.
[2] Consejo Nacional de Investigaciones Científicas y Técnicas (CONICET). Argentina.

**ICWG**

**KEY WORDS:** Iceberg, sea ice, synthetic aperture radar, edge detection

**ABSTRACT:**

The detection of icebergs in the open sea, as well as its evolution in displacement and shrinking, is vital for navigation, the study of the evolution of Polar regions, and the Earth climate change, among others. In order to carry out these studies, it is necessary to delimit accurately the icebergs in satellite images, mainly of the Synthetic Aperture Radar (SAR) type. The Adaptive Canny method has shown to be efficient for the detection of edges of objects in SAR images, according to recent publications and conferences. These studies were only carried out for images that had approximately half of each backscatter, without considering that the dimension of the objects can affect the edge detection process. Here, we present the results of the efficiency of the Adaptive Canny method as the size of the object, from which it is intended to extract the contour, decreases. A systematic analysis of the behavior of the method has been performed with objects of variated dimensions, through a Monte Carlo type experiment with synthetic images, where the contours of the figures were extracted with the Adaptive Canny method and compared with the Ground Truth (GT). Then, the method was tested on real images of the Antarctic Ocean, with blocks of ice of different sizes to contrast the results with those obtained with synthetic images.

## INTRODUCTION

The study of icebergs in the open sea is very important in the current scientific community, including their detection, monitoring, and modeling (Marino, 2018, Shui, Fan, 2018, Nunziata et al., 2018, Rupa et al., 2018, Li et al., 2019, Zakharov et al., 2019). The detection of icebergs is also of interest to monitor the ice change of the Antarctic Ice Sheet (AIS) (Whitehouse et al., 2019), and navigation safety, among others.

Many studies have shown the advantages and capacities of airborne and satellite Synthetic Aperture Radar (SAR) for iceberg detection and characterization. One of the distinguishing features of SAR images is the presence of speckled multiplicative noise that hinders the process if traditional methods for optical images are used. Due to the complexity of the noise characteristic of these images, several works address the edege detection problem in SAR images using different techniques, including artificial intelligence (Barbat et al., 2019, Li et al., 2019, Nemer et al., 2016, Nemer Pelliza et al., 2019). One of the main objectives of this research area is to detect these ice blocks and be able to track them automatically (Krieger, Floricioiu, 2017).

The Canny's algorithm is a very well known and widely implemented multistage edge detector. The extraction of coastal lines in space-borne based SAR images using this algorithm is particularly complicated because of the multiplicative speckle noise present in them and the algorithm can only be used if Cannys Parameters are appropriately chosen. The Adaptive Canny method was presented in (Nemer Pelliza et al., 2019) where, through artificial intelligence techniques, a set of functions for the calculation of these parameters to be used in SAR images are obtained, showing a high rate of efficiency in the process. Additionally, the training in almost balanced images between the two surfaces from which the contours are extracted was shown. In this paper, we analyze the efficiency of the method when the objects from which the contours must be extracted have different sizes, as is the case with blocks of oceanic ice.

The first section of this paper briefly describes the problem characteristics and the second section describes the proposed method. The third section shows the results obtained, both in synthetic images and in real images. The last section analyzes the results, provides conclusions, and proposes future works.

## 1. PROBLEM CHARACTERISTICS

This section presents the background of this work, including the characteristics of SAR images, ocean ice, and icebergs. In addition, the Canny method for edge detection and its variant here used, the Adaptive Canny method for edge detection, are explained. Finally the PFoM efficiency measurement method is described.

### 1.1 Satellite SAR image characteristics

Synthetic Aperture Radar (SAR) is an active radar that emits microwave pulses towards the Earth surface in a short period of time and, through sensors, receives echoes from reflections of the signal on objects, called backscatter. These sensors can be mounted on satellites, airborne, or on fixed antennas at high points. The SAR images used here are obtained with specialized sensors placed on satellites.

Due to the high travel speed of the space vehicle (approximately 7.5 km/s), the antenna of the SAR device becomes virtually a larger antenna. The target remains in the antenna beam for a few moments and is observed by the radar from numerous

*Corresponding author

This contribution has been peer-reviewed.
https://doi.org/10.5194/isprs-archives-XLII-3-W12-2020-459-2020 | © Authors 2020. CC BY 4.0 License.
Primary publication at IEEE Xplore: https://doi.org/10.1109/LAGIRS48042.2020.9165572

points along the satellite path, which is equivalent to prolonging the actual length of the antenna. The main advantage of using this type of image is that it can be captured despite the bad weather or lack of lighting. The intensity of a SAR image follows a negative exponential distribution and can be modeled mathematically as the product of the radar cross-section and a noise term, called speckled, which is distributed exponentially with a $\mu = 1$.

The data format (complex, intensity or amplitude) and polarization are important information to be taken into account in the statistical model, so, in this work, we follow the multiplicative SAR model of monopolarized data in intensity introduced by (Frery et al., 1997). This model proposes the following statistical distributions for the return $Z$, considering three types of texture in the backscatter,

1. Homogeneous case,

$$Z_I\left(n,\beta\right) \sim \Gamma\left(n, n/\beta^2\right) \tag{1}$$

where $\beta = \{4, 8, 12\}$. The bigger $\beta$, the smaller mean and smaller variance.

2. Heterogeneous case,

$$f_{Z_I}\left(z\right) = \frac{2\ \left(\sqrt{\lambda_1 n}\right)^{n+\alpha_1}}{\Gamma\left(\alpha_1\right)\ \Gamma\left(n\right)}\ z^{\frac{n+a}{2}}\ K_{n-a}\left(2\sqrt{\lambda_1 n z}\right) \tag{2}$$

where $\alpha = \{4, 6, 8\}$ and $\lambda = \{3, 5, 7\}$. The bigger $\alpha$, the greater mean and the bigger $\lambda$, the greater variance.

3. Extremely Heterogeneous case,

$$f_{Z_I}\left(z\right) = \frac{2n^n\ \Gamma\left(n-\alpha_2\right)\ z^{n-1}}{\Gamma\left(n\right)\ \gamma^{\alpha_2}\ \Gamma\left(-\alpha_2\right)\left(\gamma_2 + nz^2\right)^{n-\alpha_2}} \tag{3}$$

where $\alpha = \{-15, -8\}$ and $\gamma = \{1, 8\}$. The greater $\alpha$, the greater mean, and the greater $\gamma$ the smaller variance.

In all cases $n$ corresponds to the number of looks of the image. Here, $n = 1$ is exclusively used.

### 1.2 Sea ice or icebergs

The tracking of ice blocks that move on the surface is important for several scientific and navigation purposes. There are many studies that measure the ice blocks with satellite images and also are validated with ground-based radars and with measurements using GPS (Akbari et al., 2018). Icebergs protrude only one-eighth of its height from the surface, which is why they represent a serious danger for vessels since at surface level they can be avoided while they can be impacted under the surface. Icebergs are classified according to their size and shape. There are six types of icebergs depending on their size:

- **Glowler**: less than 1 meter high and less than 5 meters long.
- **Bergy Bit**: 1 to 4 meters high and 5 to 14 meters long.
- **Small**: 5 to 15 meters high and 14 to 60 meters long.
- **Medium**: 16 to 45 meters high and 61 to 122 meters long.
- **Large**: 46 to 75 meters high and 123 to 213 meters long.
- **Very Large**: more than 75 meters high and more than 213 meters long.

There are basically two types of icebergs according to their shape: tabular and non-tabular. The tabular ones are icebergs with a plateau shape, that is, steep slopes and flat tops. They are usually very large since their height/length ratio is at least 5:1. The non-tabular ones are the remaining ones and there are at least 5 sub-types: Dome, Pinnacle, Wedge, Dry dock and Blocky. The classification according to form will not be taken into account in this work.

### 1.3 Adaptive Canny's Edge detection Method

This method of edge detection was presented by (Canny, 1986), and aims to find edges while satisfying three main criteria:

- *Low Error Range*: Only existing edges must be detected.
- *Good Location*: The distance between the detected edge pixel and the actual edge pixel must be minimized.
- *Minimum response*: Only one detection response per edge pixel.

It uses a 5-stage algorithm that allows detecting borders within images:

1. *Gaussian blurring:* It eliminates part of the noise present in the image, defining each pixel as the weighted sum of the neighborhood values of $5 \times 5$ multiplied by the corresponding Gaussian weight, divided by the total weight of the mask. The neighborhood coefficients are determined according to the $\sigma$ parameter, which characterizes the Gaussians shape.

2. *Obtaining the gradient:* Detects the magnitude and orientation of the gradient vector of each pixel. The obtained image is filtered with a Sobel core in the horizontal and vertical directions to obtain two images. The first derivate in the horizontal direction is registered in an image $G_H$ and the first derivate in the vertical direction is registred in an image $G_V$. From these two images, the gradient value of the border and the direction for each pixel can be computed. The result is rounded to one of the four directions, namely horizontal, vertical and the two diagonals.

3. *Non-maximum suppression:* Refines the edges of the previous stage, eliminating the not maximum pixels that are in a predetermined environment. This step is applied until all remaining edges are one pixel wide.

4. *Threshold with Hysteresis:* Eliminates the breakage of an edge line caused by the output operator fluctuation above one threshold and below another. The process analyzes each pixel in the image, those with a value above $l_l$ are considered to be edges and are marked so. Then, the pixels connected to them with a value greater than $l_u$ will also be selected as borders. The algorithm will continue until a gradient less than $l_l$ is found.

5. *Close the contours:* This stage aims to close the contours that could have been left open due to the presence of noise.

To reach these goals, the Canny edge detector depends on three parameters, *standard deviation* ($\sigma$), *lower limit* ($l_l$) and *upper limit* ($l_u$). In (Nemer Pelliza et al., 2019) a set of formulae is proposed for the determination of these coefficients in the case of SAR satellite images. In this paper, the combination corresponding to homogeneous and heterogeneous backscatter was selected. These functions are:

$$\begin{cases} l_l = 0.4172 - 0.1219\frac{\sigma_I}{\mu_I^2} \\ l_u = 0.6250 + 0.1702\sqrt{\frac{\mu_I}{\sigma_I}} \\ \sigma_c = 1.1826 + 2.3362\frac{\sigma_I}{\mu_I} \end{cases} \quad (4)$$

Where $\mu_I$ and $\sigma_I$ are the mean and the standard deviation of the pixels values of the image.

### 1.4 Edge map quality measure PFoM

Edge map quality is a difficult quantity to measure. If Ground Truth is available, Pratt's Figure of Merit measure is a widely considered choice (Pratt, 2007). Pratt states that there are three types of errors associated with edge detection:

- Missing valid edge points.
- Failure to localize edge points.
- Classification of noise fluctuation as edge points.

The PFoM index, defined by Equation (5), balances these three types of error,

$$PFoM = \frac{1}{MAX\{I_i, I_a\}} \sum_{j=1}^{I_a} \left( \frac{1}{1 + a.d_j^2} \right) \quad (5)$$

where $I_i$ and $I_a$ represent the number of ideal and actual edge map points respectively, $a = 1/9$ is a constant scaling factor defined in (Pratt, 2007), and $d$ is the separation minimum distance from a point of the actual edge normal to a line of ideal edge points. The PFoM index scores the images with values from 0 to 1, being 1 the optimum and 0 the worst response.

## 2. PROPOSED METHOD

The technique used for the analysis is the Monte Carlo Method which consists in performing a large number of random simulations, through which complex functions can be approximated.

### 2.1 Simulations

In this paper, random images are generated with two different backscatters present in each image, a homogeneous one (Equation (1)) characterized by $\beta = 4$ for the background, and a heterogeneous one (Equation (2)) characterized by $\alpha = 6$ and $\lambda = 3$ for the objects. For both distributions, the number of looks $n = 1$ is used. These characterizations correspond to backscatter dispersions associated with water and ice. A number of 100 synthetic images with $500 \times 500$ pixels were generated for each object size and processed with the Adaptive Canny method with the set of equations in (4). Objects were defined as squares with sides ranging from 1 to 40 pixels, associated with the classification of icebergs.

The figure 1 shows 3 examples of the Adaptive Canny behavior for objects of different sizes. Images with objects much larger than those used were placed, so that they can be distinguished in the figures.

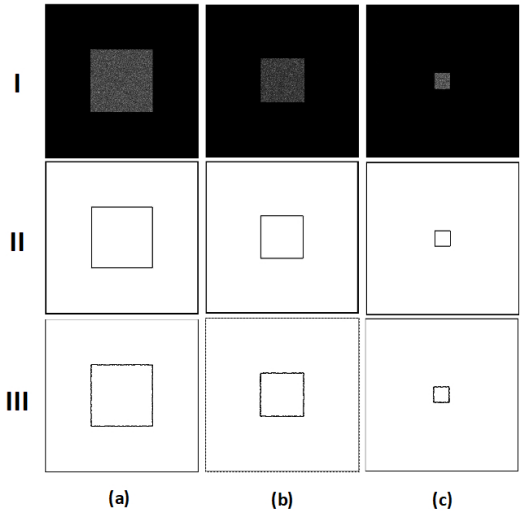


Figure 1. Synthetic images examples: (I) Noisy images, (II) GT (Ground Truth), (III) Adaptive Canny result. Images with objects of size (a) 200, (b) 150 and (c) 50.

## 3. RESULTS

### 3.1 Synthetic Images

After the simulations, the object sizes were classified according to the same criteria used for icebergs, i.e. Small, Medium, Large, and Very Large sizes. In this work we use Sentinel 1, High-resolution Level-1 GRD, and IW products, so the ice of the *Glower* and *Bergy Bit* classifications cannot be detected because each pixel has $10 \times 10$ meters of spatial resolution.

**3.1.1 Small** This classification corresponds to ice blocks between 1 and 6 pixels wide. Figure 2 shows the behavior of the Adaptive Canny's Method for this set of objects. Each of the pixels misclassified has a big influence on the PFoM due to the size of the object present in the image.

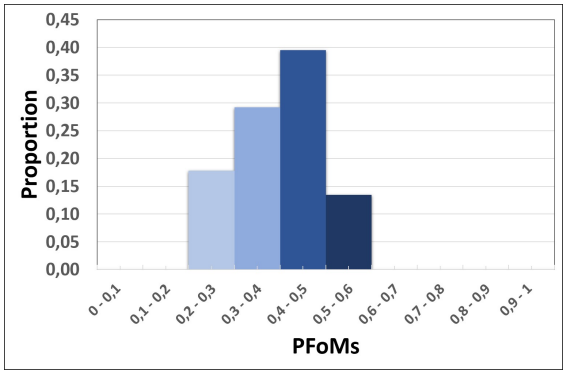


Figure 2. Histogram of proportions of PFoMs obtained with the Adaptive Canny Method for *Small* objects, from 1 to 6 pixels, both included

Figure 2 shows the PFoMs of the synthetic images processed, most of the results are above 0.4, which is not bad for the size of the objects.

**3.1.2 Medium** This classification corresponds to ice blocks between 7 and 12 pixels wide. Figure 3 shows the behavior of the Adaptive Canny's Method for this set of objects. It can be seen an improvement in the results, because more than 50% of the times the PFoMs are above 0.5.

This contribution has been peer-reviewed.
https://doi.org/10.5194/isprs-archives-XLII-3-W12-2020-459-2020 | © Authors 2020. CC BY 4.0 License.
Primary publication at IEEE Xplore: https://doi.org/10.1109/LAGIRS48042.2020.9165572

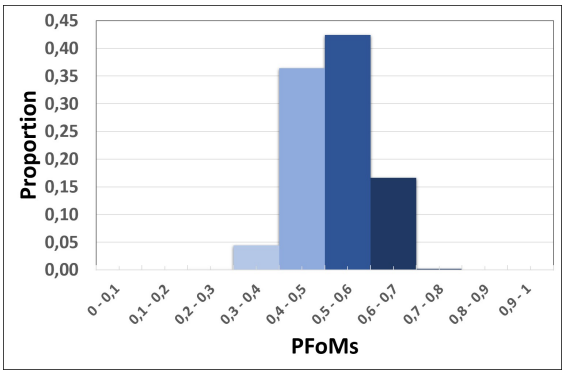


Figure 3. Histogram of proportions of PFoMs obtained with the Adaptive Canny Method for *Medium* objects, from 7 to 12 pixels, both included

**3.1.3 Large** This classification corresponds to ice blocks between 13 and 21 pixels wide. Figure 4 shows the behavior of the Adaptive Canny's Method for this set of objects. The improvement in the results is evident as the size of the objects under study increases, obtaining that in more than 40% of the cases the PFoMs are above 0.6.

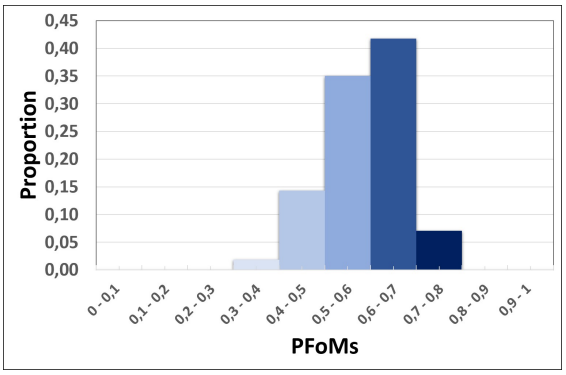


Figure 4. Histogram of proportions of PFoMs obtained with the Adaptive Canny Method for *Large* objects, from 13 to 21 pixels, both included

**3.1.4 Very Large** This classification corresponds to ice blocks between 22 and 40 pixels wide. Figure 5 shows the behavior of the Adaptive Canny's Method for this set of objects. It can be seen that almost 80% of the cases have got a PFoM above 0.7, which is a very good result.

### 3.2 Satellite SAR Images

The SAR images were downloaded through the Alaska Satellite Facility (ASF) application, Vertex. We worked with images SENTINEL-1 Interferometric Wide (IW) Swath Level 1 (ESDIS, 2019). The images were equalized and processed.
Figure 6 shows the locations of the SAR satellite images that were processed and presented in Figures 7, 8, and 9. Form each sector we have extracted a set of square-images with 500 pixels wide, with the presence of varied sizes of sea ice in them. In these figures, we show the result of applying the Adaptive Canny Method.

Figure 7 shows a large number of ice blocks as well as noise. The method extracted all the edges accurately, even on the large iceberg present on the second row, with a very complex shape.

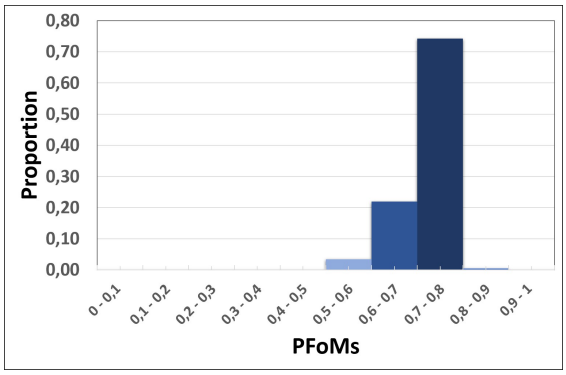


Figure 5. Histogram of proportions of PFoMs obtained with the Adaptive Canny Method for *Very Large* objects, from 22 to 40 pixels, both included

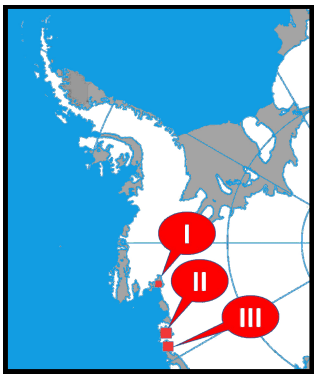


Figure 6. Antarctic sector from which the images were extracted. Square areas I, II, and III correspond to images shown in Figures 7, 8, and 9, respectivelly.

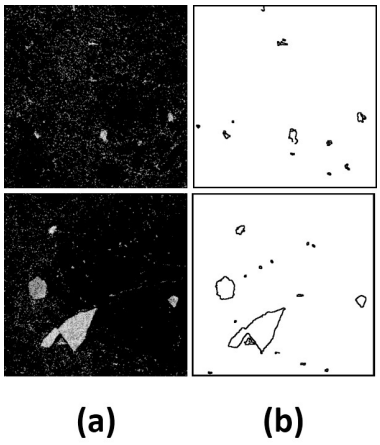


Figure 7. (a) SAR images of the areas referred to the *Sector I* in the map of Figure 6. (b) Edge detection result of applying the Adaptive Canny method.

Figure 8 shows the edge extraction in a zone with continental and sea ice, and the method maps them accurately. The speckle in the continental ice does not cause mistakes in the method.

Figure 9 shows other images with different sizes of sea ice in which edges where extracted accurately.

The precision of the edge extraction did not change from synthetic to real SAR images.

This contribution has been peer-reviewed.
https://doi.org/10.5194/isprs-archives-XLII-3-W12-2020-459-2020 | © Authors 2020. CC BY 4.0 License.
Primary publication at IEEE Xplore: https://doi.org/10.1109/LAGIRS48042.2020.9165572

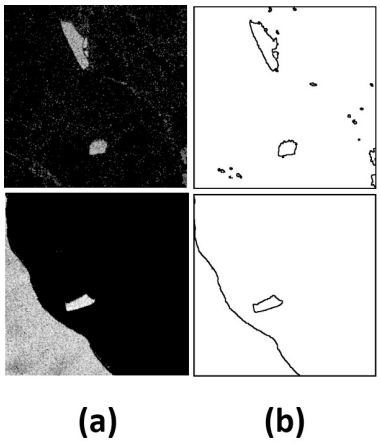


Figure 8. (a) SAR images of the areas referred to the *Sector II* in the map of Figure 6. (b) Edge detection result of applying the Adaptive Canny method.

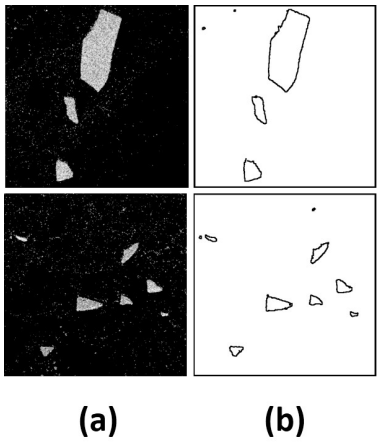


Figure 9. (a) SAR images of the areas referred to the *Sector III* in the map of Figure 6. (b) Edge detection result of applying the Adaptive Canny method.

## 4. CONCLUSION

In this work, the efficiency of the Adaptive Canny method applied to objects that are a few pixels length was analyzed. A Monte Carlo method was used to analyze synthetic images. A total of 4000 synthetic images, distributed in 100 repetitions of each of the 40 sizes analyzed, from 1 to 40 pixels, were generated. Then, the method was applied to real satellite SAR images of Antarctica in which a large variety of ocean ice and icebergs were observed and detected.

It is shown that the Adaptive Canny method works correctly in both synthetic and real SAR images, being able to efficiently detect the contour of a large variety of ice block sizes. It was also shown that the method efficiency is highly susceptible to the sea ice size that is processed.

In future works, the adaptive Canny method will be applied to detect fishing vessels in conflict zones, using higher resolution images, thus overcoming the problem of error or lack of detection in objects of a few pixels wide.

## ACKNOWLEDGMENTS

This research has been partially supported by Secyt-UTN under PID-UTN 4811TC, 4839, 7819TC and 7691 grants.

We also thanks to the Distributed Active Archive Center of the Alaska Satellite Facility for giving us permission to do research with the imagery dataset (ESDIS, 2019) here evaluated.

## REFERENCES

Akbari, V., Lauknes, T. R., Rouyet, L., Negrel, J., Eltoft, T., 2018. Validation of SAR Iceberg Detection with Ground-Based Radar and GPS Measurements. *IGARSS 2018 - 2018 IEEE International Geoscience and Remote Sensing Symposium, Geoscience and Remote Sensing Symposium, IGARSS 2018 - 2018 IEEE International*, 4623.

Barbat, M. M., Wesche, C., Werhli, A. V., Mata, M. M., 2019. An adaptive machine learning approach to improve automatic iceberg detection from SAR images. *ISPRS Journal of Photogrammetry and Remote Sensing*, 156, 247 - 259.

Canny, J., 1986. A computational approach to edge detection. *IEEE Transactions on Pattern Analysis and Machine Intelligence*, 8(6), 679-698.

ESDIS, 2019. Synthetic aperture radar imagery dataset from RADARSAT-1, CSA 2019. NASA Earth Science Data and Information System (ESDIS) project. Dataset retrieved from Alaska Satellite Facility - Distributed Active Archive Center (ASF-DAAC) on 16 Oncober 2019.

Frery, A. C., Muller, H. J., Yanasse, C. C. F., Sant'Anna, S. J. S., 1997. A model for extremely heterogeneous clutter. *IEEE Transactions on Geoscience and Remote Sensing*, 35(3), 648-659.

Krieger, L., Floricioiu, D., 2017. Automatic glacier calving front delineation on Terrasar-X and Sentinel-1 SAR imagery. *2017 IEEE International Geoscience and Remote Sensing Symposium (IGARSS)*, 2817–2820.

Li, X., Huang, W., Peters, D. K., Power, D., 2019. Assessment of Synthetic Aperture Radar Image Preprocessing Methods for Iceberg and Ship Recognition with Convolutional Neural Networks. *2019 IEEE Radar Conference (RadarConf), Radar Conference (RadarConf), 2019 IEEE*, 1.

Marino, A., 2018. Iceberg Detection with L-Band ALOS-2 Data Using the Dual-POL Ratio Anomaly Detector. *IGARSS 2018 - 2018 IEEE International Geoscience and Remote Sensing Symposium, Geoscience and Remote Sensing Symposium, IGARSS 2018 - 2018 IEEE International*, 6067.

Nemer, K. A., Pucheta, M. A., Flesia, A. G., 2016. Unsupervised fuzzy-wavelet framework for coastal polynya detection in synthetic aperture radar images. *Cogent Engineering*, 3(1).

Nemer Pelliza, K. A., Pucheta, M. A., Flesia, A. G., 2019. Optimal Canny's Parameters Regressions for Coastal Line Detection in Satellite-Based SAR Images. *IEEE Geoscience and Remote Sensing Letters, Geoscience and Remote Sensing Letters, IEEE, IEEE Geosci. Remote Sensing Lett*, 1.

Nunziata, F., Buono, A., Migliaccio, M., Moctezuma, M., Parmiggiani, F., Aulicino, G., 2018. Multi-Frequency and Multi-Polarization Synthetic Aperture Radar for the Larsen-C A-68 Iceberg Monitoring. *2018 IEEE 4th International Forum on Research and Technology for Society and Industry (RTSI),2018 IEEE 4th International Forum on*, 1.

Pratt, W., 2007. *Digital Image Processing: PIKS Scientific Inside*. 4 edn, Wiley-Interscience, John Wiley & Sons, New York.

Rupa, C., Rangarao, J., Babu, P. R., 2018. Object Based Open Sea Icebergs Identification Using Transformation Techniques. *2018 Second International Conference on Intelligent Computing and Control Systems (ICICCS), 2018 Second International Conference on*, 458.

Shui, P., Fan, S., 2018. SAR Image Edge Detection Robust to Isolated Strong Scatterers Using Anisotropic Morphological Directional Ratio Test. *IEEE Access*, 6, 37272-37285.

Whitehouse, P. L., Gomez, N., King, M. A., Wiens, D. A., 2019. Solid Earth change and the evolution of the Antarctic Ice Sheet. *Nature Communications*, 10, 2041-1723.

Zakharov, I., Puestow, T. P., D. Howell, M., 2019. Icebergs in Sea Ice With TanDEM-X Interferometry. *IEEE Geoscience and Remote Sensing Letters, Geoscience and Remote Sensing Letters, IEEE, IEEE Geosci. Remote Sensing Lett.*, 1070.

This contribution has been peer-reviewed.
https://doi.org/10.5194/isprs-archives-XLII-3-W12-2020-459-2020 | © Authors 2020. CC BY 4.0 License.
Primary publication at IEEE Xplore: https://doi.org/10.1109/LAGIRS48042.2020.9165572